

Study On the Performance of Concrete Tunnel Systems Subject to Fault Displacement

¹VISHWAJEET TOPPO,²Dr.RAGHVENDRA SAHU

¹PG SCHOLAR, ²ASSISTANT PROFESSOR,

¹Department of CIVIL ENGINEERING,

¹GIET UNIVERSITY, GUNUPUR, INDIA

Abstract: A Finite Element Analysis (FEA) investigation of concrete tunnel systems traversing seismic faults is carried out to determine how to effectively mitigate the stresses induced in the liner when subject to fault displacement. A parametric study of various fault parameters, both in the damage zone and competent rock, is carried out to determine the site conditions which induce the most stress on the tunnel liner system. Results indicate that friction angle, cohesion, and elastic modulus of fault zones have varying effects on the stresses induced on the liner. The width of damage zone and expected displacements are also investigated and it has been shown that even small displacements over narrow damage zones, around 10 m, can still result in significant damage to the concrete liner whereas in wider damage zones the effects of the displacement are more evident. The use of flexible joints in what is known as the articulated design method is investigated to mitigate the stresses induced by fault displacement and discussed. Several orientations, lengths and variations in relative stiffness of these flexible joints are investigated to determine their optimal effectiveness. Results show that this is an effective solution which can be used in design and repair of tunnels to mitigate the stresses and resulting damages to concrete tunnel liners subject to fault displacement.

1.INTRODUCTION

General:

Tunneling is a large industry, from the underground construction of transportation tunnels to relieve surface congestion to lifeline systems required to provide essential utilities. Although avoided, if possible, it becomes inevitable that some of these systems will cross faults in seismically active regions. This is a problem in areas such as the state of California which is a well-documented, seismically active area, namely due to the San Andreas Fault system in southern California. Tunnels in these regions are not only subject to dynamic loading from earthquakes, but those which cross active faults are also subject to a large degree of fault dislocation. Stability, strength and serviceability immediately become issues as the tunnel is forced to deform with the fault, which can cause major damage to the concrete tunnel liner. Figure 1.1 illustrates the damage to tunnel liners due to the shear deformations imposed by the surrounding ground. The mitigation of damage to tunnel liners caused by fault dislocation is the focus of this research.

1.1 Tunnels & Background of Tunneling

Tunnels are constructed in a multitude of ground conditions varying from soft clays to hard rocks and the method of construction is highly dependent on these ground conditions as well as other factors, such as groundwater conditions, depth of tunnel and diameter of the tunnel. Today, there are three general methods of tunnel construction: cut- and-cover tunneling, immersed tunneling, and bored tunneling as depicted by Figure 1.2. In this research the latter method is of most concern as cut-and-cover and immersed tunnels are not subject to fault displacement to the same degree as bored tunnels. The methods of tunneling described herein, are not meant to be an exhaustive detailing or design procedure of each method, but rather a succinct description of the approach and evolution of each method. It should be noted the methods described here are not the only methods of tunnel construction used in practice.

1.2.1 Cut & Cover Tunnels

The opening of America's first subway system – only two miles long – was achieved in 1897 due to the new technique at the time, known as cut and cover (Roach et al. 2017). In this method of tunnel construction, a trench is cut into the ground where the tunnel box is framed, and then covered which allows activities at the surface to continue while the final adjustments to the tunnel are made underground, depicted in Figure 1.3. Albeit an impressive achievement at the time, this subway system was quickly overshadowed in 1904 by New York's 21-mile subway system project designed by William Barclay Parsons, whose firm (Parsons Brinkerhoff) improved and refined the cut- and cover method throughout the twentieth century (Roach et al. 2017). This method is well-proven technique for the construction of shallow tunnels reaching 15 meters in depth (up to 30 meters is possible but requires much more support structures) and is commonly used in constructing tunnel portals (Mohammed 2014).

1.2.2 Immersed Tube Tunnels

In lieu of a bridge, or where bridge construction is not possible, an immersed tube tunnel construction method is a viable technique to cross rivers or other bodies of water. As the name implies, this method consists of floating prefabricated, water-tight, tunnel sections into place, and lowering each section into trenches that are dredged out of the river or seabed before being backfilled (Bickel et al. 1996). The

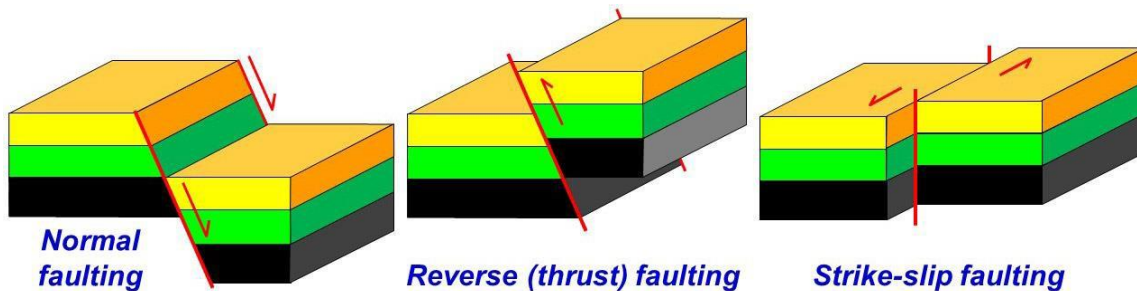
use of this technique was first adopted to transport sewage underneath the Boston Harbor by the means of an iron tube known as the Shirley Gut Siphon (Figure 1.4), constructed in 1896 (Lotysz 2010). Some fifteen years later, The Michigan Central Railway Tunnel, the first immersed tunnel to carry traffic, was constructed beneath the Detroit River connecting Detroit, Michigan with Windsor, Ontario (Lotysz 2010). Bickel et al. (1996) cites that this method of tunnel construction is the most economically inexpensive option for crossing bodies of water, under favorable conditions.

1.2.3 Bored Tunnels

Although the earliest forms of mechanized tunneling were developed throughout the 1800s, it was not until 1952 that modern tunneling techniques were realized when James Robbins completed the Oahe Dam diversion project in South Dakota with the use of his rock tunnel boring machine shown in Figure 1.5 (Roach et al. 2017). The further evolution of tunnel boring machines (TBMs) that propelled tunneling into the modern era was the development of rotating cutterheads and shields. TBMs are often used in bored tunnel construction because they make it possible to accommodate tunnels at great depths as well as a wide variety of diameters. A very well detailed development of TBM technology throughout history can be found in pertinent literature (Roach et al. 2017)

1.3 Faults & Faulting

A fault is break in the rocks of the Earth's crust where there is relative movement on either side of the discontinuity. This movement can happen very slowly over time as rocks move and deform past one another or very suddenly when a fault ruptures and an earthquake



ensues. In areas of repeated faulting, instead of a single discrete break, fault zones are formed and are composed of smaller regions of parallel or branching faults usually separating masses of broken rock (Davis et al. 2012). The wider the fault zone, the more displacement imposed on the zone, in general (Davis et al. 2012). The fault plane is the flat surface of the fault which defines the blocks on either side of the fault. Fault planes are typically not oriented 90 degrees to the horizontal plane, and the angle between these planes is defined as the dip. When this fault plane is not vertical (90 degrees), the block of fault immediately below the fault plane is defined as the footwall and the block above is referred to as the hanging wall. The net slip of a fault is defined as the movement of the hanging wall relative to the footwall, parallel to the fault plane. The lateral component of the net slip is known as the strike-slip and the vertical component is known as the dip-slip, as shown in Figure 1.12 (Davis et al. 2012). There are three main types of faults, as shown in Figure 1.13, which develop under different states of stress and are generally classified by the type of movement across the fault plane. However, it should be noted that there are other types of faults characterized by a combination of movements, stresses and also rotations. The first category of faults is normal faults, which are faults formed under tension and extension causing the hanging wall to move downward relative to the footwall in response to gravity (Earle 2015). Normal faults are often found at divergent plate boundaries, where parts of the Earth's crust are being pulled apart. Faults formed under compressive stresses are reverse faults, and their movements are characterized by the hanging wall moving upwards relative to the footwall (Earle 2015). Reverse faults are characteristic at convergent plate boundaries where one tectonic plate is subducted beneath the other as they are compressed together. Schematics of a normal fault, reverse fault and strike-slip fault (KGS at the University of Kentucky) (Used by permission)

Rocks transformed during faulting can be thought of as brittle or ductile fault rocks, each formed depending on the deformation's mechanisms of faulting or shearing present, although the specific nature of fault rocks depends also on starting materials and fault conditions (Davis et al. 2012). Brittle fault rocks are formed under frictional sliding and cataclasis, which is defined as "the pervasive brittle fracturing and granulation of rocks, generally along faults and fault zones," by Davis et al. (2012). These brittle fault rocks can be further organized as incohesive brittle fault rocks (breccias) and cohesive brittle fault rocks (cataclasites). The former is normally formed within the top of the Earth's crust, within a depth of about 4 km, whereas the latter is formed when temperature and strain rates are right, usually at greater depths (Davis et al. 2012). Accordingly, ductile fault rocks are formed under ductile deformation mechanisms of faulting and shearing such as ductile dislocation creep. Conditions for ductile flow of rock is commonly at great depths with high temperatures and pressures, except for weak rocks with can undergo ductile deformations at relatively shallower depths were temperature and pressure are not as great (Davis et al. 2012). The conditions in which these rocks normally form are similar to that of the formation of metamorphic rocks and have similar characteristics, both containing foliations, parallel alignments of planar fabric elements of rock, and metamorphic minerals. However, these types of rocks are distinguished from metamorphic rocks and are called tectonites or assigned mylonitic rocks (Davis et al. 2012).

2.OBJECTIVE AND SCOPE:

The primary objective of this thesis is to investigate the effectiveness of the articulated design method in mitigating stresses in the tunnel liner system and resulting damages due to fault displacement. The scope of this work is accomplished using Finite Element Analysis (FEA) software, specifically ANSYS Workbench, to investigate tunnel- fault interaction. Using ANSYS, properties of the competent rock and damage zone of the fault are parametrically studied to determine critical parameters which induce the most damage on the tunnel liner. Using the critical parameters identified, the effectiveness of flexible joints in the articulated design method are investigated using different orientations, lengths, and relative stiffnesses to determine the most effective way to implement flexible joints into a tunnel liner system.

3.LITERATURE:

Introduction

The studies presented in this section outline methods of modeling faults, surrounding ground, tunnel structures and fault displacements for investigating tunnels that traverse active fault zones.

3.1 FEM of Faults & Surrounding Ground

This section will describe several aspects and methods of modeling faults, soil and rock properties for the purposes of accurately capturing tunnel-fault interaction necessary to develop the parametric relationships required for this research. This section is primarily organized from the simpler modeling of soil behavior to more detailed methods of modeling. This is specifically done to highlight the complexities and intricacies of soil behavior and to reinforce the difficulties in accurately modeling this behavior. In fact, **Ladd et al.** (1977) summarizes this point quite well,

“The ideal soil behavior model would describe the soil’s deformation and pore pressure response under all types of loading conditions at any time, strength being incorporated as an upper limit to the stress-strain relationship ... A generalized model of the stress-strain behavior of soils should ideally account for nonlinearity, yielding, variable dilatancy (volume changed cause by shear stress), and anisotropy (both inherent and stress system induced), plus the behavioral dependence on stress path, stress system (orientation of σ_1 and relative magnitude of σ_2), and stress history (both initial and changes due to consolidation).” – pg. 454

Russo et al. (2002) discusses fault crossing strategies for twin shield tunnels (specifically for the Bolu Tunnel project) crossing the **Bakacak Fault and the Zekidađi Fault** in Turkey. In 1999, after the **Düzce** earthquake (MW = 7.2), a detailed seismic reconnaissance of the area around the Bolu Tunnel project was carried out, allowing for a more accurate modeling of the two faults for the study. The **Zekidađi** Fault dips approximately 90 degrees with the tunnel crossing this fault over the length of 25 to 30 m (82 to 98 ft.) in both tubes. . This fault was identified with low potential for future rupture with an estimated right lateral offset displacement of 0.15 to 0.25 m (5.91 to 9.84 in) from an associated earthquake with magnitude MW from 6 to 6.25. The **Bakacak** Fault dips approximately 40 degrees with the tunnel crossing this fault over the length of 100 m (328 ft). Estimated rupture displacements are up to 0.5 m (19.69 in) from an associated earthquake with magnitude MW from 6.25 to 6.5. Fault ruptures may occur in a concentrated or a distributed manner, and for the **Bakacak** Fault it was assumed – then justified by geologists, that its displacements would most likely be distributed and mainly horizontal whereas the displacements at the **Zamindari** Fault could not be accurately predicted. Because of this previous assumption, the researchers were able to assume the shear strain in the fault soil as the ratio between expected offset and width of the fault at tunnel level. The soil was modeled as Mohr- Coulomb (M-C) compression springs using contact elements between the tunnel liner and soil.

Daller & Weigl (2011) investigated concepts for the new **Semmering Base Tunnel** in Austria to find a support and construction process which would provide tunnel displacements compatible with the fault system using FLAC2D. This tunnel was constructed through the **Graßberg-Schlagl** fault system and rock characteristics for this system were determined by triaxial compression tests from core samples. The results from a triaxial compression test on one specimen was back-calculated using the finite element program ZSoil, considering the Hardening Soil (HS) – Small Strain constitutive law as well as the M-C constitutive law to help determine the relevancy of a nonlinear analysis. **Obrzud** (2010) discusses the significance of using the HS model as opposed to the M-C model in ZSoil and ultimately concluded that the HS model is the more accurate model to use in finite element analysis. The linear-elastic M-C model does not always give reliable and realistic predictions in FEA because soil is only truly elastic at very small strains. The HS- Standard Model considers the pre-failure non-linearities of soil behavior while reproducing basic macroscopic phenomena exhibited by soils such as densification, stress dependent stiffness, soil stress history, plastic yielding and dilatancy (**Obrzud** 2010). Moreover, the advanced version of this model, the HS-Small Strain model, incorporates the above phenomena along with strong stiffness variation as well as the hysteretic, nonlinear elastic stress-strain relationship of a soil (**Obrzud** 2010). **Obrzud** (2010) reanalyzed the tunnel excavation of the twin Jubilee Line Extension Project in London, UK using HS models as well as the M-C model to prove that the HS models give more realistic stress-strain behavior of the soil by comparing results to triaxial lab tests (Figure 2.1). Figure 2.1a shows that at very small strains (< 0.01% axial strain) the HS-Small and M-C Models accurately model the behavior captured during isotropically consolidated undrained extension (CIUE) tests. However, in Figure 2.1b it can be seen that at larger strains, the HS-Model is what actually captures the soil’s behavior across the range of strains expected. In fact, the HS- Small model used by **Daller & Weigl** (2011) also agreed well with lab data constructed from triaxial compression tests compared to the M-C model which did not accurately fit to the data.

Daller & Weigl (2011) also had access to cross-sections of this fault system from a railway project in May of the previous year and were able to generate a forecast model of the section of the fault under concern which consisted of six vertical rock bodies. This information

also provided the strikes and dips of the faults although the authors decided to convert all of the fault planes to 90 degrees for simplification purposes. The authors conclude that an improvement to this study should include a three-dimensional analysis of an improved model of the geologic structure as well as more in-situ and laboratory testing of core fault material; however, the study does prove the shortcomings of the M-C model at large strains.

Ohbo et al. (2000) conducted a study to analyze the seismic performance of a shield tunnel that crosses an active fault with significantly different ground on either side of the fault. The authors conducted two-dimensional finite element dynamic analyses.

In tunnel-fault research done by **Shahidi and Vafaeian (2004)**, the fault displacement was determined by assuming the differential deflection to be Δ . Ground behavior and soil-structure interaction were modeled under the conditions of two-dimensional plane strain elastic-plastic criterion. The physio-mechanical properties of the faulted zones were varied linearly from the center of the fault zone to the boundaries on both sides of the fault. Based on seismic analysis, the Zarab fault with a dip of 85° will be displaced approximately 0.37 m along a distance of 300 m. A basic assumption of the calculations is that 85% of the differential deformation occurs along a zone of 15 m within the center of the faulted zone.

Luo & Yang (2013) performed a finite element analysis using ABAQUS to see the effects on a tunnel by a dislocation of faults. The model consisted of bedrock, concrete lining and fault fractured zones

Wang et al. (2012) used FLAC3D to model tunnels crossing active faults subjected to a differential displacement across the fault. A fault zone, as opposed to a discrete fault plane, was modeled and the fault displacement was estimated to be 0.2 m. However, the width of the modeled fault zone was not specified, although a finite thickness can be

assumed from Figure 2.4, which shows a profile of their tunnel-fault model in FLAC3D. The tunnel liner is modeled using three dimensional elastic elements and ground behavior was modeled using the M-C criterion. Wang et al. (2012) found that under strike-slip conditions, the damage to surrounding rock and tunnel liner were more serious than that of the other fault conditions analyzed, thus their flexible joint design is based on strike-slip conditions.

Shahidi and Vafaeian (2004) present a method of designing a flexible lining for tunnels within the regions of active faults for the particular case of a shield tunnel located in Iran crossing two faults of concern: the **Zarab Fault and the Naaleshkenan Fault**.

Russo et al. (2002) present similar design philosophies and principles and applied this to the Bolu Tunnel project as part of the North Anatolian Motorway in Turkey. The twin tunnel project crosses the Bakacak Fault and the Zekidaği Fault; however, the Zekidaği Fault had already been driven by the time this report was released. The authors assume, similar to assumptions made by Shahidi and Vafaeian (2004) that the tunnel will behave as an embedded concrete beam whose extremities are subject to the displacement of the fault.

In the research by **Luo & Yang (2013)**, they investigated three segmented tunnels, each containing only one segment using lengths of 5, 10 and 15 m, and one continuous tunnel (no segments). All tunnels were modeled with an ideal elastic-plastic constitutive model. Their goal was to study the stress and deformation of the tunnel structures under fault dislocation, which averaged 0.5 m, applied vertically to the hanging wall of their model. For the contact surface between the two walls a friction coefficient of 0.3 was defined and the friction coefficient at the contact surface between the ground and tunnel liner was defined as 0.7. The plastic zone in the tunnels was noted to be reduced when the tunnels were modeled as segmented structures.

Orzud (2010) and Ohbo et al. (2000) both modeled their tunnel structures using beam elements, likely because their respective studies were more heavily focus on the modeling of the ground surrounding the tunnel and not the actual performance of the liner itself. Ding et al. (2006) modeled their tunnel using an eight-node hexahedron solid element in their modeling of the tunnel's response to seismic excitation.

4. FINITE ELEMENT MODELING

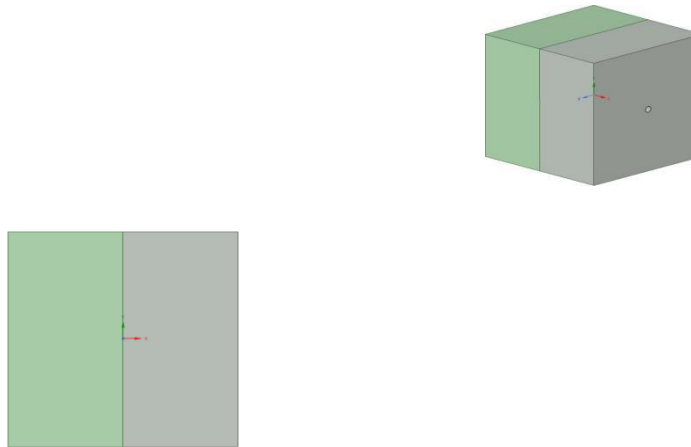
4.1 Introduction

This chapter describes the methods of modeling the tunnel and surrounding ground for preliminary elastic analysis as well as nonlinear analysis. Geometries (tunnel and ground), meshing, boundary conditions and mechanical properties are all outlined in this chapter. Concrete behavior of the tunnel liner is represented using the Hognestad (1951) material model of unconfined concrete to account for the nonlinearity in the stress-strain behavior of concrete. Equations are included to also modify the behavior of plain concrete to represent the behavior of fiber-reinforced concrete. Effort is also made to account for the nonlinear, anisotropic, stress-dependent behavior of soil and rock included in this modeling.

Geometry

The three-dimensional geometries for tunnels, fault zone and surrounding ground were created using SpaceClaim3D design modeling software built into the ANSYS Workbench program. Using this software allowed for easy integration into the ANSYS program for finite element analysis. In preliminary analysis, the foot wall and hanging wall of the fault are identically sized rectangular prisms (100 m x 50 m x 100 m) placed together to result in a fault zone modeled by 3D solid elements. The two walls of the fault meet at the fault plane with a dip of 90°, and this plane is where the entirety of the fault dislocation occurs. This geometry was created for the sole purpose of preliminary, linear analysis to determine how to apply displacements and check if the distribution of stresses throughout the model made sense before moving onto nonlinear analysis. There are also models created where distributed displacements will be applied. This is done by including a third rectangular prism in between the two walls of

the fault, the damage zone, where distributed displacements across the width of the damage zone will be applied. Per pertinent literature discussed in Section 2.2, three additional geometries were created with damage zones of 10 m, 50 m, and 100 m (32 ft, 164 ft, and 328 ft) which can be seen in Figure 3.2. In these models, widths of the footwall and hanging wall are held constant at 50 m (164 ft). The reason that the widths of the competent rock (footwall and hanging wall) are held constant is because results from preliminary analysis show there is no significant boundary influence on stresses using widths of 50 m from where the fault displacement is applied.

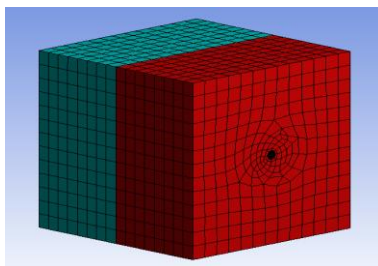


- plan view of ground and fault geometry where the green highlighted body is the footwall and the light gray body is the hanging wall of the FEM. b) shows location of tunnel in elevation, passing through the fault.
- The tunnel used in this modelling is a 5.0 m outer diameter tunnel liner, D , with a liner thickness of 0.5 m, t , also modelled as 3D solid elements. The tunnel has a length of 100 m, L , which extends through the entirety of the ground modelled. An isolated view of the tunnel geometry is shown in Figure

The tunnel length chosen to be used in analyses is important because after the simulated fault dislocation, there should be negligible effects from dislocation at either end of the tunnel such that the total effect of fault displacement is captured in the model. A tunnel length of 100 m was chosen for the tunnel in creating the single fault plane model and the analyses remained computationally inexpensive with respect to time of analyses. The center of the tunnel lies 50 m from ground surface and also 50 m perpendicular to the parallel planes of the ground, as shown in Figures 3.1 and 3.2. The preliminary tunnel geometry is modeled as one continuous, hollow cylinder extending through the fault as shown in Figure 3.3. In the geometries where damage zones are included, the tunnel length is adjusted to run through the width of the surrounding ground, spanning through the entirety of the hanging wall, damage zone and footwall. In 10 m damage zone geometries where segments are introduced, the individual segments are separated by 1 m and 5 m links to allow for the tunnel to bend with the fault displacements applied. These individual segments may not always have continuous reinforcement running throughout but are modeled as continuous segments because the concept is to force weak points in the tunnel liner, where much of the displacement will occur, into the links between segments. Figures 3.4 and 3.5 are included to show the articulated geometries used to investigate a damage zone width of 10 m where links are located at either end of damage zone. Figures 3.6 3.11 show the 100 m articulated geometries. These are different configurations of 5 m and 1 m links investigated in Section 4.3 to determine the effectiveness in the articulated design method. Geometries 100-1 and 100-b have links where the damage zone meets the competent rock and 100-2 and 100-2b have links on either side. Geometries 100-3 and 100-3b are like 100-1 and 100-1b, but fully articulated through the damage zone.

4.2 Meshing

An effective mesh is important in this analysis to provide accurate results without becoming too computationally expensive. The Automatic Meshing feature within ANSYS resulted in an effective mesh meeting these criteria. The mesh used is a rectangular mesh for both the tunnel and ground with a mesh refinement value of 1 over the entire model. The rectangular meshed elements appear regular away from the tunnel and begin to change shape into irregular, angular shapes which decrease in size closer to the modeled tunnel. Figure 3.12 and 3.13 show the meshing of the ground and tunnel, respectively. During nonlinear analysis, the mesh will be refined in the area immediately surrounding the fault zone to gain more accurately capture the behavior of the tunnel liner subjected to fault displacement.



Automatic meshing of the ground surrounding the tunnel. The light blue body is the footwall and the red body indicates the hanging wall. In the 10 m damage zone liner has a total of 6,420 elements and 43,802 nodes.

The 50 m damage zone liner contains 5,568 elements and 37,770 nodes. The 100 m damage zone liner has a total of 5,355 elements and 34,522 nodes. In further analyses, the meshing on the tunnel is refined using the “Body Sizing” feature in ANSYS Workbench, to increase the number of elements spanning the cross-section of the tunnel liner to be greater than 1 element thick, so that more accurate distributions of stresses and strains could be measured through the cross-section in determining failure of the concrete liner. To determine the appropriate body sizing for the tunnel liner, a mesh convergence study was performed to determine the optimal mesh size by converging on a target of 5% convergence. The meshing for the surrounding ground is left automatically meshed because in this research the concern is studying the stress distributions in the tunnel liner, not the ground

5. RESULTS

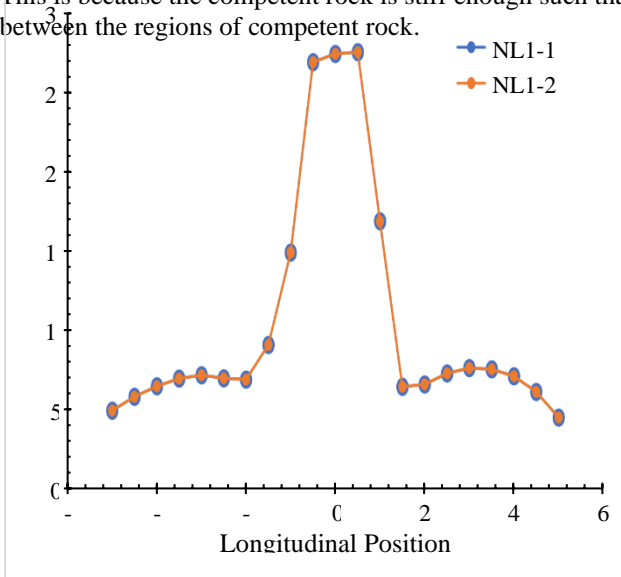
5.1 Effects of Competent Rock Properties

Models run in this section show that the competent rock behaves linearly with the applied displacement of 1 m and although the stresses in the rock may change when nonlinear controls are turned on, the stresses induced in the nonlinear tunnel liner remain the same. The lowest reasonable value for elastic modulus in competent rock is about 2,000 MPa and for the damage zone the lowest reasonable value is about 50 MPa. Using a 10 m damage zone model where the elastic modulus of the damage zone and competent rock as described above along with 0.2 value for Poisson’s Ratio was applied. From pertinent literature discussed in Sections 2.4 and 3.5, the lowest reasonable cohesion value for competent rocks is about 6.7 MPa which was also applied to the competent rock in the models. The initial inner friction angle in the competent rock and damage zone were set to 40° and 30°, respectively, typical values from literature. The ratios for residual friction angle and dilatancy angle to initial inner friction angle are set at 0.5 and 1.0 for both rocks. The range of cohesion values in damage zone rock ranges from 0.1 MPa up to 1.0 MPa and are also tested to prove linearity in competent rock. The ratio of residual cohesion to initial cohesion is 1.0 for both rocks as well. Table 4.1 presents the properties of the two models, NL1-1 and NL1-2, just described.

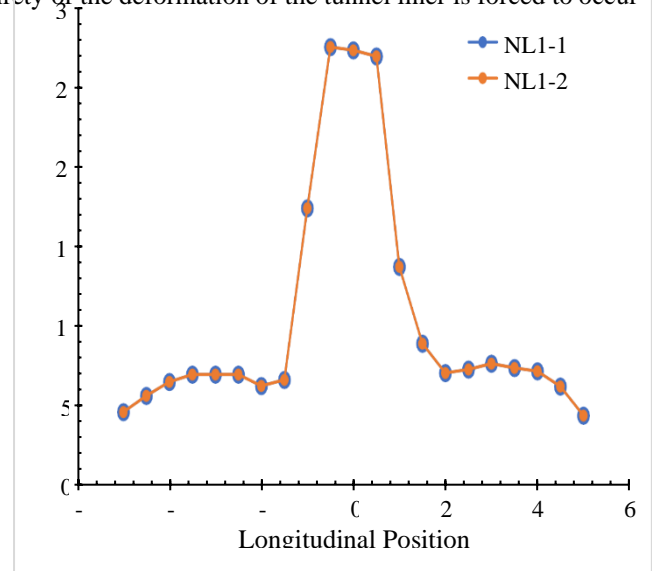
5.2 Elastic Response of Competent Rock

It should be noted that in this chapter the stresses plotted in figures are the maximum stresses measured in the entire region of the crown or invert of the tunnel. To start, a model was run with nonlinearity turned on in both competent rock and damage zone rock and then run again with nonlinearity only in the damage zone rock. This research proves that if there is no difference in stresses induced in the tunnel liner between the two identical models that the competent rock behaves linearly and nonlinearity does not have to be turned on in the competent rock which, as described above, reduces computational expenses without compromising accuracy of the results. The results which are presented are the Von-Mises stresses and normal longitudinal stresses induced in the tunnel liner by the applied fault displacements. The maximum Von-Mises and normal stress at 5 m increments along the longitudinal position of the tunnel, for both the crown and invert of the tunnel, is graphed in plots to show how the distribution of stresses changes along the length of the tunnel. Figures 4.1-4.4 show these plots for models NL1-1 and NL1-2 where the only difference between the two models is that the competent rock is run without nonlinear controls turned on for the latter model. These figures show that the lines for Von- Mises stress and normal stress for both the crown and invert of the tunnel liner plot

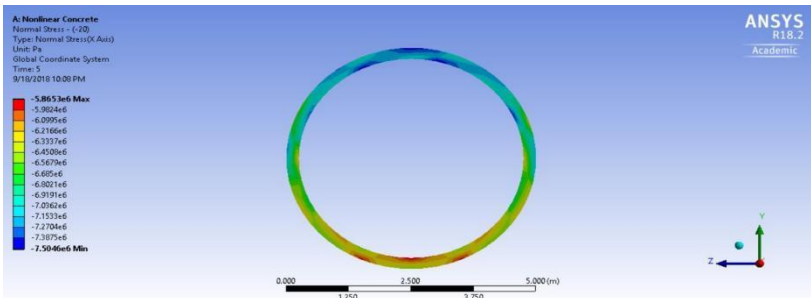
directly on top of each other which prove that the competent rock behaves linearly even when nonlinear controls are turned on for the competent rock. To further show this, tunnel cross sections at these 5 m increments of normal stress and Von-Mises stress for these two models are included in Figures 4.5-4.16. Only one half of these are shown because the other half of the tunnel is symmetric as shown in plots. These visually show how the distribution is exactly the same throughout the tunnel liner. Figures 4.17 and 4.18 are also included to show how the displacements of the tunnels in these two models are also exactly the same. These figures show that the deformations are localized through the 10 m damage zone and constant in the competent rock regions. This is because the competent rock is stiff enough such that the entirety of the deformation of the tunnel liner is forced to occur between the regions of competent rock.



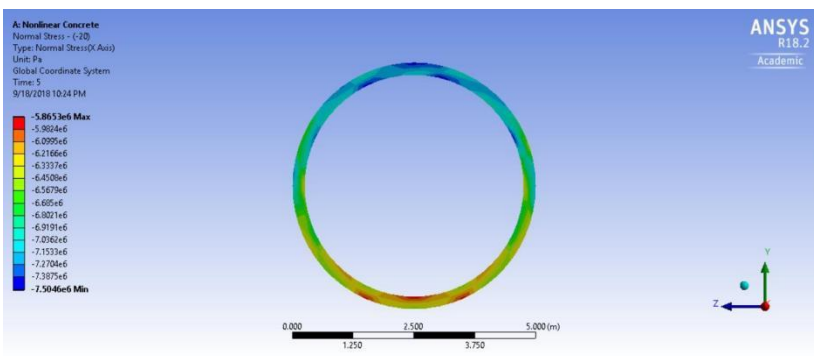
Plot of maximum Von-Mises stress in tunnel crown for NL1-1 and NL1-2.



Plot of maximum Von-Mises stress in tunnel invert for models NL1-1 and NL1-2.



-20 m normal stress in the x-axis of the tunnel liner of model NL1-1.



-20 m normal stress in the x-axis of the tunnel liner of model NL1

5.3 Cohesion & Friction Angle in Competent Rock

To determine if the value of initial cohesion defined in the competent rock affects the model results, cohesion was increased to 10 MPa in model NL1-3 to see if results change. Figures 4.19-4.22 show that increasing the cohesion did not affect the stresses induced in the tunnel liner which indicates that the cohesion is high enough in the competent rock such that the rock will always behave linearly, within the range of reasonable values of cohesion tested. The properties of the models in these figures are presented in Table 4.2. The initial inner friction angle is changed to a low, reasonable value for intact rock, 15° in model NL1-5. The results from changing the initial inner friction angle from to a low value and comparing it to a model where the initial inner friction angle of the competent rock is at a high value, 50° in model NL1-4 proving that nonlinearity in the competent, intact rock is controlled by the value of initial cohesion, and since it is proven that the minimum value used does not invoke nonlinearity in the models even when the initial inner friction angle is varied, the competent rock can be run linearly.

5.4 Elastic Modulus of Competent Rock

The elastic modulus of competent rock was then investigated. All properties for the models described, NL1-6 & NL1-7. Similar to the plots shown above, the distribution of Von-Mises and normal longitudinal stresses displayed in these graphs plot on top of one another which indicates that the competent rock still behaves linearly even when the elastic modulus is increased to a high value as determined from literature. This also means that its behavior is still controlled by the defined value of initial cohesion. Also, when the elastic modulus of the competent rock is increased from 2,000 MPa up to 100,000 MPa the maximum value of stress throughout the tunnel liner embedded in the competent rock is significantly increased from 7 MPa to 19 MPa although the stresses within the damage zone remains unaffected. The even distribution of stresses in the 100,000 MPa competent rock.

Damage Zone Length

Additional models were run to study damage zones greater than 10 m in width. The damage zone was set to 100 m and analyses are done like NL1-1 through NL1-7. Figures 4.31-4.34 show that even when nonlinearity is introduced into the competent rock of model NL2-1 but excluded from NL2-2, similar to the 10 m damage zone, the lines of stress plot on top of one another proving that the competent rock behavior remains linear with the applied displacements even when the lowest possible initial inner friction angle and initial cohesion are tested (15° and 6.7 MPa, respectively). Full properties of the rock can be found in Table 4.5. Figures 4.35 and 4.36, are included to show the directional deformation of NL2-1 and NL2-2, respectively, to visually represent how the tunnel would deform over a 100 m damage zone

Effects of Damage Zone Properties

This section presents the findings from investigating the effects of damage zone properties of the 10 m damage zone on the stresses induced on the concrete tunnel liner. This is followed by the investigation of the damage zone properties of the 100 m and 50 m damage zones and related back to the findings made for the 10 m damage zone.

Cohesion in Damage Zone

The effects of nonlinearity in the damage zone is investigated. Figures 4.45-4.48 are presented to show how the range of values of initial cohesion affects the distribution of stresses in the tunnel liner where the competent rock properties are identical throughout the three models. Table 4.8 presents the properties of the rocks used in these models. It should be noted that the model where the damage zone initial inner friction angle is set to 15°, it had difficulty completing successfully so knowing that using a value of 30° works, a model was created using a value of 40° such that a trend could be recognized. 40° will not be used in final modeling, just to get a trend for the effect of friction angle. Figures 4.45 and 4.46 show that as the value of initial cohesion increases, the distribution of Von-Mises stresses decreases away from the damage zone but within the damage zone, the difference in results is negligible. In the plots of normal stresses, Figures 4.47 and 4.48, the same is true and the normal stresses in the crown and invert of the tunnel liner decreases as the value of initial cohesion of the damage zone is increased. This means that low cohesion damage zone rocks have greater affects in increasing the stresses in the tunnel liner into the competent rock zone. Although this is evident, because the stresses induced are less than about 10.3 MPa (1,500 psi), these stresses are not considered critical enough that the sections of the liner systems in the competent rock require additional design to mitigate stresses and to prevent damage if they are properly designed.

Elastic Modulus of Damage Zone

In determining the 10 m damaged zone elastic modulus critical to the models, initial cohesion of 0.1 MPa and initial inner friction angle of 30° are used as the M-C properties in the damage zone. In investigating the effects of varying initial cohesion in models where the damage zone and competent rock elastic moduli are 50 MPa and 100,000 MPa, respectively, the effect of elastic modulus in the competent rock overtakes the effects of varying cohesion and friction angle in the competent rock. This means that the competent rock is stiff enough that it moves as a rigid body with the applied displacement, carrying the tunnel within it, and creating an even distribution of high stresses throughout the liner in the competent rock, about 19.3 MPa (2,800 psi), regardless of the effects of friction angle and cohesion as described in Sections 4.2.1 and 4.2.2. This is shown in Figures 4.59 and 4.60, where only these two plots are shown because of the symmetry which exists in the crown and invert of the tunnel liner. Properties of the models shown in those plots are presented in Table 4.10. With the higher elastic modulus of the competent rock to save computational expenses, a cohesion value of 0.3 MPa could effectively be used in modeling in place of cohesion value of 0.1 MPa because results between the two cohesion values are equivalent as seen in Figures 4.45 – 4.48. It was also found that

when using the elastic modulus value in the damage zone higher than 50 MPa it is found that the models cannot complete the runs entirely before failing. This is because the stiffnesses of 500 MPa and 5,000 MPa are so stiff compared to the concrete liner, that the movement of the rock forces so much stress into the concrete, that the liner fails completely before being able to displace the full 1.0 meter. It was found that in 500 MPa and 5,000 MPa rock, the liner can displace about 6.5 and 0.7 cm respectively.

Displacement Effects

The effects of varying displacement are investigated to determine if stress distributions are significantly altered before reaching the full 1.0 m displacement applied to critical models. Figure 4.69 and 4.70 show the Von-Mises and Normal stress distributions for the 10 m damage zone with applied displacements of 5 cm, 25 cm and 1.0

m. Figures 4.71 – 4.76 show the associated stress distributions from ANSYS. For this width of damage zone, even small displacements create high, critical stresses within the damage zone. These stresses are high enough that they need to be addressed in design.

The 100 m critical damage zone is also investigated for the same effects of varying displacement. The plots of stress distributions as well as the associated stress distributions from ANSYS are shown in Figures 4.77 – 4.84. Different from the 10 m damage zone, the effects of varying displacement have a greater influence of stress distributions. It is evident in these plots that as the displacements are increased, the stresses are significantly increased in the liner. Low displacements are not as critical in the 100 m damage zone as they are in the 10 m damage zone.

Articulated Design Method

To lessen the damage incurred by the concrete tunnel liner due to fault displacement, the articulated design method as a solution was investigated and discussed in this section. The articulated design strategy was investigated in the critical models determined for the 10 m and 100 m damage zones.

For the 100 m damage zone, six different articulated design methods were investigated for their effectiveness.

The relative stiffness ratio of steel used in these models is 1/50. The stress distributions throughout the tunnel are also shown in Figures 4.87 – 4.89 and 4.92 – 4.94. The maximum stresses both inside and outside of the damage zone are slightly increased but not enough to cause significant damage in the tunnel liner however the fully segmented geometries, Geometry 100-3 and Geometry 100-3b, result in the most favorable stress distributions, that is, no significant amount of damage occurs in the concrete of the liner system. In addition, the stress distribution in the immediate vicinity of the faulting is significantly decreased from the continuous liner system presenting a favorable and constant stress distribution throughout the damage zone. This indicates that the links in the tunnel liner system allow the stresses to favorably redistribute as the links of the tunnel system concentrate hinging through the fault. The results also show that there is no significant difference in stress distributions between the corresponding 5 m and 1 m links for any given orientation of link placement. It is shown that the lowest relative stiffness ratio in the linked section results in the most favorable stress distribution throughout the liner by limiting the stresses that can be developed in the hinges. This is shown visually through Figures 4.97 and 4.98 and comparing to Figure 4.89. Through investigating the 10 m articulated geometries, it was found that the concrete tunnel still experienced significant damage under the applied 1.0 m fault displacement using a relative stiffness ratio of 1/10. FEA using relative stiffness ratios of 1/20 and 1/50 for Geometry 10-1 can only go through 52.3 cm and 37 cm, respectively. Using the same ratios for Geometry 10-2 can both go through 37.3 cm of fault displacement.

6. SUMMARY & CONCLUSIONS:

Parameters of competent rock and damage zone rock properties were studied to observe their effects on tunnel liner damage. The use of articulated tunnel liners to mitigate liner damage was also evaluated. A literature review was completed to determine appropriate ranges of material properties and fault displacements.

Results show that competent rock can be modeled as linear-elastic using only the elastic properties for up to 1.0 m fault displacement investigated, and for the properties gained from literature review. It was also determined the M-C properties of the damage zones have effects of varying degrees. In 10 m damage zones subject to 1 m of fault displacement, surrounded by softer competent rock ($E = 2,000$ MPa), the effects of the cohesion and friction angle of the faulted rock are evident in the stress distribution of the tunnel liner outside of the damage zone into the competent rock though full yielding of the liner in the damage zone was observed for all cases. Higher friction angle and lower cohesion result in the highest stress values in the competent rock section of the tunnel. These stresses do not have a critical enough impact such that special care and design be undertaken to mitigate these stresses. However, in cases where the faulted rock is surrounded by stiffer competent rock ($E = 100,000$ MPa), it is the elastic properties of the competent rock that control the stress distributions in the tunnel liner outside of the damage zone instead of the M-C properties of the faulted rock in the damage zone. So, it is recommended that special care be taken to accurately measure the M-C properties in short damage zones surrounded by soft rock so that they can be accurately modeled to determine stress distributions throughout the tunnel liner, however this is not as critical in damage zones surrounded by hard rock. But in hard rock, special care should be taken in measuring the elastic properties, so it can be determined if the stresses into the competent rock are critical enough for the given design such that they can be designed for expected fault displacement. In long damage zones, around 50 m in length and greater, lower cohesion and higher friction angles of the damage zone rock create slightly higher stress

values in the portion of the tunnel liner crossing the damage zone. However, these M-C properties are less critical than in the shorter damage zone of 10 m investigated. The portion of the tunnel liner outside the damage zone, in the competent rock, the stress distributions are controlled by the elastic properties of the competent rock. In damage zones of these lengths and greater it is likely that the elastic properties of the rock are what dominate the stresses induced in the tunnel liner outside of the damage zone. It seems that as the damage zone increases in length, the M-C properties of the damage zone become less important in determining the stress distribution in the tunnel liner. Models with elastic moduli of the damage zone greater than 50 MPa can only undergo a fraction of the displacement that it can in softer ground. Special care should be taken in stiffer damage zones to evaluate stress distributions in the tunnel liner caused by fault displacements as they could only withstand smaller fault displacements in the FEA. Investigating the use of the over-excavation method as a possible solution to allow these tunnels to move through expected fault displacements is suggested